Environmental Science & Technology

Article

Cite This: Environ. Sci. Technol. 2018, 52, 4099−4107

pubs.acs.org/est

# Proton and Copper Binding to Humic Acids Analyzed by XAFS Spectroscopy and Isothermal Titration Calorimetry

Jinling Xu,[†,‡] Luuk K. Koopal,[§,∥] Linchuan Fang,[*,†] Juan Xiong,[§] and Wenfeng Tan[*,†,§]

[†]State Key Laboratory of Soil Erosion and Dryland Farming on the Loess Plateau, Institute of Soil and Water Conservation, Chinese Academy of Sciences and the Ministry of Water Resources, Yangling, Shaanxi Province 712100, P. R. China

[‡]University of Chinese Academy of Sciences, Beijing, 100049, P. R. China

[§]College of Resources and Environment, Huazhong Agricultural University, Wuhan 430070, P. R. China

[∥]Physical Chemistry and Soft Matter, Wageningen University and Research, Stippeneng 4, 6708 WE Wageningen, The Netherlands

Supporting Information

**ABSTRACT:** Proton and copper (Cu) binding to soil and lignite-based humic acid (HA) was investigated by combining X-ray absorption fine structure (XAFS) spectroscopy, isothermal titration calorimetry (ITC), and nonideal-competitive-adsorption (NICA) modeling. NICA model calculations and XAFS results showed that bidentate and monodentate complexation occurred for Cu binding to HA. The site-type-specific thermodynamic parameters obtained by combining ITC measurements and NICA calculations revealed that copper binding to deprotonated carboxylic-type sites was entropically driven and that to deprotonated phenolic-type sites was driven by entropy and enthalpy. Copper binding to HA largely depended on the site-type and coordination environment, but the thermodynamic binding mechanisms for Cu binding to the specific site-types were similar for the different HAs studied. By comparing the site-type-specific thermodynamic parameters of HA−Cu complexation with those of low molar mass organic acids, the Cu coordination could be further specified. Bidentate carboxylic−Cu complexes made the dominating contributions to Cu binding to HA. The present study not only yields molecular-scale mechanisms of ion binding to carboxylic- and phenolic-type sites of HA but also provides the new insight that the universal nature of site-type-specific thermodynamic data enables quantitative estimation of the binding structures of heavy metal ions to humic substances.

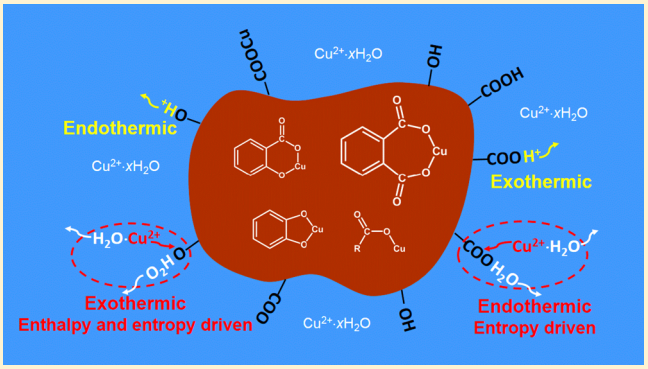


## 1. INTRODUCTION

Humic substances (HS) represent on average 70%−80% of the natural organic matter and play a key role in regulating metal ion speciation because of their strong affinity for metal ions.[1] The most important components of HS in relation to ion binding are fulvic acid (FA) and humic acid (HA); FA and HA are operationally defined natural organic particles that differ in size and solubility, but both contain various types of acidic functional groups that can interact with protons and metal ions.[2,3] Due to the important role of HS in controlling the bioavailability of metal ions in nature, metal ion−HS systems have been extensively investigated, see for example, refs 2 and 4−6.

Metal ion binding to HS and the metal ion chemical speciation can be best described by models that take the site heterogeneity, site competition, and electrostatic interactions explicitly into account; in this way, the binding parameters are intrinsic properties independent of the solution conditions. Model V/VI/VII[7−9] and the nonideal-competitive-adsorption (NICA)−Donnan model[10,11] address these aspects.[12−14] An advantage of the NICA−Donnan model is that the final result is an analytical binding equation that can be applied relatively easily to measured data sets using standard software.[15−18] Once the NICA−Donnan model parameters are known, practical insight into metal ion binding under various conditions can be obtained by direct calculations[19] and/or by using conditional affinity spectra.[20−22] A further advantage of the NICA−Donnan model is that for specific solution conditions the binding equation can be easily simplified.[23] For instance, at constant high ionic strength, the electrostatic interactions are relatively weak, so that no electrostatic model is required and the NICA−Donnan model reduces to the NICA model. The remaining weak electrostatic interactions are in this case incorporated as pseudo-heterogeneity in the affinity distribution that are now semi-intrinsic, i.e., NICA applies at the given ionic strength, but

Received: December 6, 2017
Revised: March 8, 2018
Accepted: March 9, 2018
Published: March 9, 2018






DOI: 10.1021/acs.est.7b06281
Environ. Sci. Technol. 2018, 52, 4099−4107

the heavy metal ion speciation as a function of the pH can be calculated. Working at relatively high ionic strength in the form of a 1−1 background electrolyte has the further advantage that the diffuse ion binding is dominated by the 1−1 electrolyte, so that the diffuse heavy metal ion binding can be neglected.

The combination of measured adsorption isotherms and modeling efforts should preferably be complemented with further experimental evidence on the metal ion binding to improve and/or verify the modeling results. Such evidence can be achieved with various techniques, for instance, $^{13}C$ NMR spectroscopy,[24] fluorescence spectroscopy,[25,26] IR-ATR spectroscopy,[26] X-ray absorption fine structure (XAFS) spectroscopy,[4] or isothermal titration calorimetry (ITC).[27,28] In the present study, NICA modeling of proton and copper binding to a soil HA and a lignite-based HA is complemented with XAFS and ITC measurements. XAFS provides the averaged coordination environment of metal ions at relatively high metal loadings. ITC measurements in combination with adsorption isotherm data and NICA modeling provide the *site-type-specific (either carboxylic site-type or phenolic site-type)* thermodynamic characteristics of proton and metal ion binding to HA. The measurements are carried out at relatively high ionic strength (0.1 mol/L) to suppress the electrostatic interactions. This has the advantage that (i) the NICA model can be used (see above), (ii) a direct comparison can be made between the NICA and the ITC results, and (iii) it allows comparison of the derived thermodynamic parameters with those of low molar mass organic acids.

Thermodynamic characteristics of Cu binding to HA samples of different origins have been investigated before,[27−29] but only the average thermodynamic parameters of the *overall* binding could be obtained, and this thwarts the interpretation because averages of ion binding characteristics over two different site-types (carboxylic and phenolic) were obtained. For a deeper insight into $H^+$ and $Cu^{2+}$ binding to heterogeneous HA, *site-type-specific* information is essential and this can be obtained by using the calibrated NICA model. The site-type-specific *average* molar enthalpies ($\Delta H_j$), Gibbs energies ($\Delta G_j$), and entropies ($\Delta S_j$) of $H^+$ and $Cu^{2+}$ binding to sites of type $j$ provide information on the interactions that drive the ion binding to the specific site-types and give insight into the intrinsic differences in ion binding to the carboxylic- and phenolic-type sites; they therefore contribute to a better understanding of the binding.

The objectives of the present study are 4-fold: (1) To investigate the coordination environment of Cu binding to HA by XAFS and to compare the spectroscopic results with the (material-specific) stoichiometry indicators obtained with the NICA model. (2) To obtain the site-type-specific thermodynamic quantities ($\Delta G_j$, $\Delta H_j$, $\Delta S_j$) of proton and copper binding to HA by combining the ITC results with the speciation calculated with the calibrated NICA model. (3) To use the site-type-specific molar enthalpies and entropies to gain insight into the driving forces for proton and Cu binding to HA. (4) To compare the site-type-specific thermodynamic parameters of proton and copper binding to HA with those of low molar mass organic acids containing carboxylic and phenolic groups and to determine which structure types (combinations of sites) may be responsible for Cu binding.

## 2. MATERIALS AND METHODS

**2.1. Preparation of HA.** Soil HA was extracted from the upper horizon of a brown soil (Alfisols) in Tonghua, Jilin province (N 41°30′, E 125°55′) in China and marked as JLHA. It was isolated and purified following the standard procedure of the International Humic Substances Society.[30] Aldrich humic acid (CAS 6813-04-4) purified by the method described by Vermeer et al.[31] and denoted as PAHA was used for comparison. Stock solutions of 2 g/L were prepared at pH ≥10 with KOH and equilibrated for 24 h and then stored in the dark at 4 °C. Characterization of the two samples and proton and copper binding have been described in detail in previous studies.[22,32] For the present purpose, the data were refitted with the NICA model, and the resulting fits and parameters, as well as the model description, are shown in the Supporting Information (SI, Table S1 and Figures S1−S3).

**2.2. X-ray Absorption Fine Structure (XAFS) Spectroscopy.** The HA−Cu samples were prepared at pH 6.0 and high Cu concentrations; a high bound amount was selected in order to obtain reliable XAFS information. Copper K-edge X-ray absorption spectra of the HA−Cu samples and reference materials [CuO powder and 0.01 mol/L $Cu(NO_3)_2$ solution] were measured at room temperature on the 1W1B beamline at the Beijing Synchrotron Radiation Facility (BSRF). The XAFS spectra for HA−Cu samples and the 0.01 mol/L $Cu(NO_3)_2$ solution were collected using the fluorescence mode; the CuO powder was measured in the transmission mode. The detailed process of sample preparation and data collection is presented in the SI.

The EXAFS spectra were analyzed using the IFEFFIT software package.[33] In the data reduction step, replicate spectra were aligned to a common energy scale and averaged. From each average spectrum, a polynomial pre-edge function was subtracted, and the data were normalized. In extracting the $\chi(k)$ function, the XAFS signal was isolated from the absorption edge background by using a fit to a cubic spline function. The $k^3$-weighted $\chi(k)$ function was then Fourier transformed over the interval 2.9−12.2 $Å^{-1}$ to yield the radial structure function (RSF). Data fitting was done in $R$ space with a multishell fitting routine. The theoretical scattering phases and amplitudes used in data analysis were calculated with the FEFF 7.0 code,[34] using an input file based on a structural model of Cu(II)−phthalate.[35] The amplitude reduction factor ($S_0^2$) was determined to be 0.75, based on the fit of the CuO spectral data. With the analysis, the atomic separation distance ($R$), the coordination number (CN), and the Debye−Waller factor ($\sigma^2$) of the atom backscatters were obtained.

**2.3. Isothermal Titration Calorimetry (ITC).** The heats of proton and Cu binding to HA were measured using a TAM III (Thermometric AB) isothermal microcalorimeter and titrating protons or Cu ions into a HA solution. Prior to a titration, the HA solution was purged with $N_2$ gas to remove possible $CO_2$. All titrations were carried out at 25 °C under stirring at a rate of 120 rpm. For each proton and copper titration, an analogous titration was performed outside the calorimeter in which the pH was monitored using a combined pH-reference electrode (Metrohm, 6.0262.100). With the protonation experiments, 0.7 mL of 0.8 g/L HA in 0.1 mol/L $KNO_3$ was titrated by 20 injections of 10 μL of 0.028 mol/L $HNO_3$; the acid concentration was calibrated with sodium carbonate. The addition rate at each injection was 1 μL/s and the time interval between the injections was 10 min. The initial pH of the HA solution was about 10, and the final pH of the titration was around 3. In the Cu titration experiments, 25 sequential doses of 10 μL of 5 mM $Cu(NO_3)_2$ were added into 0.7 mL of 0.8 g/L HA solution at an initial pH of 4.0 or 5.0. The pH was adjusted to the desired $pH_{init}$ (init: initial) values by the


DOI: 10.1021/acs.est.7b06281
Environ. Sci. Technol. 2018, 52, 4099−4107

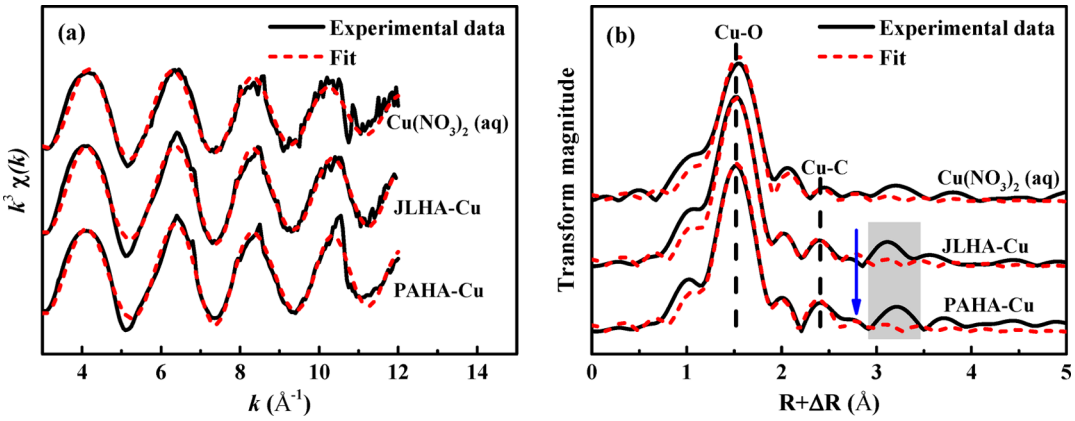


**Figure 1.** $k^3$-Weighted (a) and Fourier-transformed (b) EXAFS data (uncorrected for phase shifts) for 0.01 mol/L aqueous $Cu(NO_3)_2$ and for Cu binding to JLHA and PAHA at pH 6.0. Black solid lines represent experimental data and red dashed lines the best fit of the data.

addition of 0.025 mol/L $HNO_3$ or 0.025 mol/L KOH. For each titration, the output signal, power ($\mu$W) versus time (s), was recorded by the TAM assistant software. Each injection of titrant leads to a peak in the signal and the heat ($\mu$J) per injection was obtained by integrating the area under each peak.

The net heat of binding at the $x$th injection of titrant ($Q_x^{net}$) was obtained by subtracting the background heat ($Q_x^b$) that was measured with the blank (b) titration, from the experimentally measured heat ($Q_x^{exp}$):

$$Q_x^{net} = Q_x^{exp} - Q_x^b \quad (1)$$

With the proton titration, the heat of acid−base neutralization was also calculated from the measured pH change for each step of the titration at alkaline condition and was included in $Q_x^b$. The enthalpy of this reaction was estimated by Gorman-Lewis et al.[36] to be −56.48 kJ/mol. For the calculation of *average molar* enthalpies of H or Cu binding to the site-types of HA, the net heat of interaction has to be complemented with information on the adsorbed amount and the sites that participate in the binding.

**2.4. Thermodynamic Analysis.** With proton binding the thermodynamic analysis was as follows. With known initial pH, HA amount, as well as the solution volume and added H at a given titration step, the equilibrium site-type-specific speciation (amounts of H bound to the carboxylic- and phenolic-type sites) at the initial situation and at each step $x$ of the titration can be calculated with the calibrated NICA model. The difference in proton speciation between the start of the H-titration and step $x$ provides the change in proton speciation. The average molar enthalpy of proton binding, $\Delta\bar{H}_{HL_j}$, to the deprotonated site-types, $L_j$ ($j$ = 1, carboxylic-type sites; $j$ = 2, phenolic-type sites), can now be obtained with eq 2

$$\sum_{x=1}^{n} Q_x^{net} = \sum_{j=1}^{2}\sum_{x=1}^{n} \Delta\bar{H}_{HL_j}\Delta n_{HL_{j,x}} \quad (2)$$

where $\Delta n_{HLj,x}$ is the *change* in the total amount of H bound (mol/kg) to $L_j$ after step $x$ of the titration. The molar enthalpies are average values because both the carboxylic- and phenolic-type sites are chemically heterogeneous. Taking only one average value per site-type is a simplification, but in this way the two site-type-specific molar enthalpies can be compared with the two (semi)intrinsic affinities. The $\Delta n_{HLj,x}$ values were used as calculated and the molar enthalpies of H binding to the groups were optimized by minimizing the difference between corrected heats and calculated heats with the 1stOpt software.

To obtain the site-type-specific average enthalpies of Cu binding to JLHA and PAHA at $pH_{init}$ 4.0 and 5.0, the same procedure was followed as described for the H binding. However, with Cu binding, analysis of $Q_x^{net}$ is more complicated because $Q_x^{net}$ includes in this case two parts: one due to dissociation of protons from protonated sites that participate in the Cu binding ($HL_j = L_j + H$) and the other due to Cu binding to deprotonated site-types ($L_j + Cu = CuL_j$; charges and stoichiometry not indicated). With the above calculated molar enthalpies of H binding to the two site-types and all the bound amounts (H and Cu) calculated with the NICA model, the average molar enthalpies of Cu binding to the deprotonated site-types can be obtained by fitting the measured (corrected) heats to the calculated heats using eq 3

$$\sum_{x=1}^{n} Q_x^{net} - \sum_{j=1}^{2}\sum_{x=1}^{n} \Delta\bar{H}_{HL_j}\Delta n_{HL_{j,x}} = \sum_{j=1}^{2}\sum_{x=1}^{n} \Delta\bar{H}_{CuL_j}\Delta n_{CuL_{j,x}} \quad (3)$$

where $\Delta\bar{H}_{CuLj}$ represents the average molar enthalpy of copper binding to deprotonated sites $L_j$. The values of $\Delta n_{HLj,x}$ and $\Delta n_{CuLj,x}$ are the changes in the total amounts of species $HL_{j,x}$ and $CuL_{j,x}$ at step $x$, respectively. Therefore, the values of $\Delta n_{HLj,x}$ and $\Delta n_{CuLj,x}$ were calculated using the measured pH at each titration step. The two unknown enthalpies were fitted with 1stOpt software.

The thermodynamic analysis further requires the calculation of the site-type-specific average molar Gibbs energies and entropies. The site-type-specific average molar Gibbs energies of binding ($\Delta\bar{G}_j$) can be calculated with eq 4 using the average equilibrium binding constants, $\bar{K}_j$

$$\Delta\bar{G}_j = -RT \ln \bar{K}_j \quad (4)$$

where $R$ is the gas constant and $T$ the absolute temperature. The averaged equilibrium binding constants for proton and Cu binding to the carboxylic- and phenolic-type sites can be approximated by the site-type-specific affinities obtained with the NICA modeling: $\bar{K}_j = \tilde{k}_j$ (peaks of the distribution). The $\tilde{k}_j$ values are close to the average binding constants because the distribution function is close to symmetrical.

With the known values of $\Delta\bar{G}_j$, $\Delta\bar{H}_j$, and $T$, the site-type-specific average entropy contributions, $T\Delta\bar{S}_j$, and the site-type-



DOI: 10.1021/acs.est.7b06281
Environ. Sci. Technol. 2018, 52, 4099−4107

**Table 1. EXAFS Fitting Results of Aqueous $Cu(NO_3)_2$ and HA−Cu Complexes**

| sample | atom backscatter | $R$ (Å)[a] | CN[b] | $\sigma^2$ (Å$^2$)[c] | $\Delta E_0$ (eV)[d] | $R_f$[e] |
|---|---|---|---|---|---|---|
| $Cu(NO_3)_2$(aq) | Cu−O | 1.96 | 4[f] | 0.004 | 4.70 | 0.0006 |
| JLHA−Cu | Cu−O | 1.95 | 4[f] | 0.003 | 2.76 | 0.0004 |
| | Cu−C | 2.81 | 1.7 | 0.005 | | |
| PAHA−Cu | Cu−O | 1.94 | 4[f] | 0.003 | 2.84 | 0.0001 |
| | Cu−C | 2.85 | 1.9 | 0.004 | | |

[a]Atomic separation distance. [b]Coordination number. [c]Debye−Waller factor. [d]Energy shift. [e]Residual fraction = $\sum k(k^3x_{exp} - k^3x_{calc})/\sum k(k^3x_{calc})$, which measures the quality of the Fourier-filtered model contribution ($x_{calc}$) with respect to the experimental contribution ($x_{exp}$). [f]Parameter fixed in the fitting routine. The amplitude reduction factor ($S_0^2$) was set to 0.75.

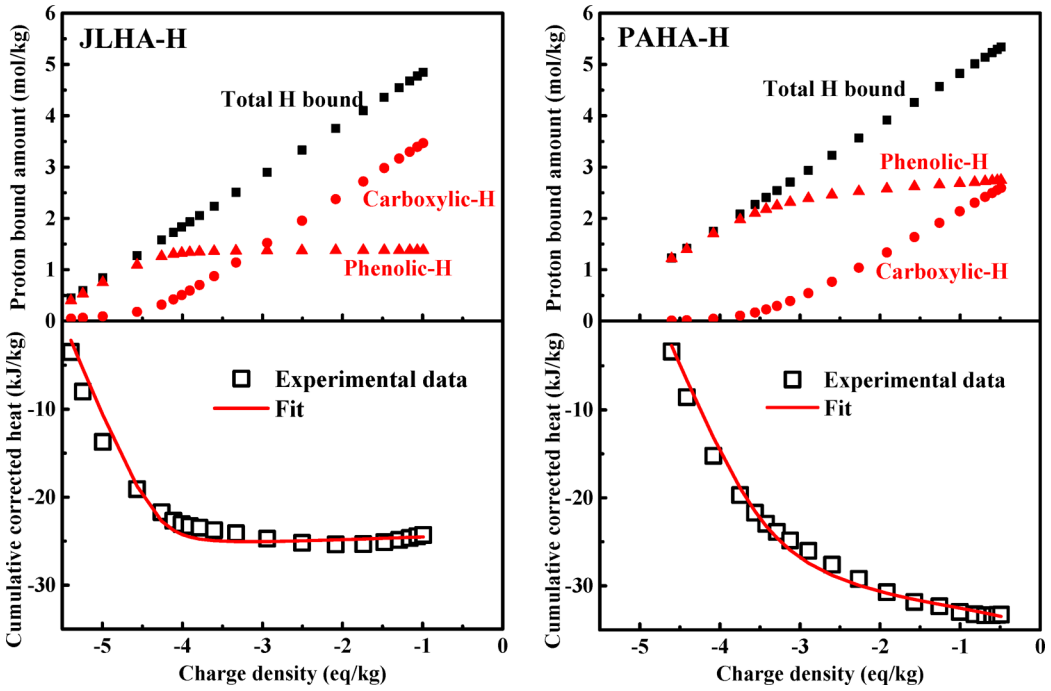


**Figure 2.** Amounts of carboxylic-H (solid red spheres), phenolic-H (solid red triangles), and total H bound (solid black squares), see the top panels, and the cumulative corrected heats (open black squares, bottom panels) as a function of the charge density (eq/kg). The symbols in the bottom panels are the experimental data and the lines the fitted data.

specific average molar entropies, $\Delta\bar{S}_j$, can be calculated by using eq 5:

$$\Delta\bar{G}_j = \Delta\bar{H}_j - T\Delta\bar{S}_j \quad (5)$$

## 3. RESULTS

**3.1. XAFS Analysis for Cu Binding to HA.** The EXAFS spectra for Cu binding to HA at pH 6.0 in 0.1 mol/L $KNO_3$ and for aqueous $Cu(NO_3)_2$ samples (both in $k$ and $R$ space) are depicted in Figure 1. The Fourier transforms of the EXAFS spectra (Figure 1b, uncorrected for phase shifts) of HA−Cu samples are similar to those of Cu adsorption onto Elliot HA.[37,38] Studies of well-defined compounds using EXAFS have shown that Cu is usually 6-fold-coordinated in the first shell, with four O atoms ($Cu-O_{eq}$) at distances of 1.90−1.97 Å, which are positioned in the equatorial plane of a Jahn−Teller distorted octahedron, and two axial O atoms ($Cu-O_{ax}$) at 2.15−2.78 Å.[39−42] The $Cu-O_{eq}$ distances of the first shell are somewhat larger for aqueous Cu than for HA−Cu, as the left vertical dashed line in Figure 1b. The vertical dashed line on the right in Figure 1b shows the peak position of the second shell for HA−Cu; this peak is absent for aqueous Cu and corresponds with the Cu−C coordination and a Cu−O−C structure.

To gain insight into the average binding environment of Cu to HA, the EXAFS spectra are fitted to a Cu−phthalate structure.[35] In the fitting routine, the $Cu-O_{ax}$ is disregarded due to its minimal EXAFS contributions, high disorder, and the closeness of bond distance to that of the more intense $Cu-O_{eq}$ backscatterers.[42] The coordination numbers (CN) of the first shell are fixed to 4. The fitted parameters of the HA−Cu complexes are listed in Table 1. The results demonstrate that the $Cu-O_{eq}$ bonds of the first shell are 1.95 and 1.94 Å for JLHA−Cu and PAHA−Cu, respectively. The second shell is fitted with 1.7 C atoms at 2.81 Å for JLHA−Cu and 1.9 C atoms at 2.85 Å for PAHA−Cu.

**3.2. Thermodynamic Parameters for Proton Binding to HA.** The calorimeter responses of the isothermal proton titrations of background electrolyte and HA solutions are presented in Figure S4 (SI). After the heat correction with blank heats, the accumulated heats of proton binding (kJ/kg) to each HA are obtained and depicted in the bottom panels of Figure 2 vs the (primary proton) charge density (eq/kg) calculated with the NICA model at each titration step. Note that this charge density is directly proportional to the amount


DOI: 10.1021/acs.est.7b06281
Environ. Sci. Technol. 2018, 52, 4099−4107

of bound protons. In the top panels of Figure 2, the corresponding proton speciation (carboxylic-H and phenolic-H in mol/kg) calculated with the NICA model is depicted. The speciation results show that at first the protonation mainly occurs on the high-affinity phenolic-type sites and then the low-affinity carboxylic-type sites. The cumulative corrected heats in the bottom panels of Figure 2 show a sharp increase of the exothermic heat when mainly the phenolic-type sites are titrated and a rather weak exothermic heat effect upon the titration of mainly the carboxylic-type sites. The weak decrease of the exothermic heat at the end of the titration is due to some slightly endothermic heat peaks at the last few proton injections. A detailed fit of the experimental heat data to eq 2 with one average molar enthalpy of proton binding to each site-type is shown in the bottom panels of Figure 2 by the red curves. The fitted site-type-specific average molar enthalpies are collected in Table 2. Both for JLHA and PAHA, the calculated site-type-specific average molar enthalpies of proton binding to the carboxylic-type sites are weakly positive (endothermic) and those to the phenolic-type sites are relatively strongly negative (exothermic).

**Table 2. Thermodynamic Parameters for Proton Binding to HA**[a]

| sample | species | $\log \tilde{k}_{HLj}$ | $\Delta\bar{G}_{HLj}$ (kJ/mol) | $\Delta\bar{H}_{HLj}$ (kJ/mol) | $T\Delta\bar{S}_{HLj}$ (kJ/mol) |
|---|---|---|---|---|---|
| JLHA | carboxylic-H | 4.47 | −25.50 | 0.20 | 25.70 |
| | phenolic-H | 9.31 | −53.11 | −23.61 | 29.50 |
| PAHA | carboxylic-H | 4.66 | −26.58 | 0.77 | 27.35 |
| | phenolic-H | 9.21 | −52.54 | −21.41 | 31.13 |

[a]The log $\tilde{k}_{HLj}$ values correspond with the affinities of the two peaks of the proton affinity distribution. $\Delta\bar{G}_{HLj}$, $\Delta\bar{H}_{HLj}$, and $\Delta\bar{S}_{HLj}$ represent the average value of Gibbs energy, enthalpy, and entropy of proton binding to sites of type $j$, respectively. The $R^2$ of the fit to obtain the enthalpies is 0.987 and 0.994 for proton binding to JLHA and PAHA, respectively.

The site-type-specific average molar Gibbs energies of proton binding ($\Delta\bar{G}_{HLj}$) are calculated using the log $\tilde{k}_{HLj}$ values; the results are also collected in Table 2. The calculated $\Delta\bar{G}_{HLj}$ values are all negative (−25.50 to −53.11 kJ/mol) because proton binding is a spontaneous process. With the known values of $\Delta\bar{G}_{HLj}$ and $\Delta\bar{H}_{HLj}$, the values of $\Delta\bar{S}_{HLj}$ are calculated with eq 5, as shown in Table 2. The positive $\Delta\bar{S}_{HLj}$ values (86.24−104.46 J/mol/K) derived from $T\Delta\bar{S}_{HLj}$ (25.70−31.13 kJ/mol) in Table 2 indicate that protonation of the HA site-types is an entropically favorable process. Decomposing the Gibbs energy into its enthalpic and entropic contribution allows a better understanding of why these reactions occur and the strength of the bonds formed. Two elementary reactions are included in ion binding to HA: dehydration of ions and HA ligands (endothermic, positive entropy) and forming carboxylic/phenolic-ion bonds (exothermic, negative entropy).[29] The protonation of carboxylic-type sites is weakly endothermic, implying that on the whole the negative enthalpy of formation of carboxylic-H cannot counteract the positive enthalpy of water loss upon proton association. For proton binding to phenolic-type sites, the negative enthalpy of formation of phenolic-H is large enough to make the reaction exothermic. Positive entropy changes in the dehydration reactions are always large enough to compensate for the negative entropy changes of complexation for both carboxylic- and phenolic-type sites, and the net entropy change of complexation is positive. Summarizing, the protonation of carboxylic-type sites is driven by entropy, while both enthalpic and entropic contributions cause the strong protonation of phenolic-type sites and the

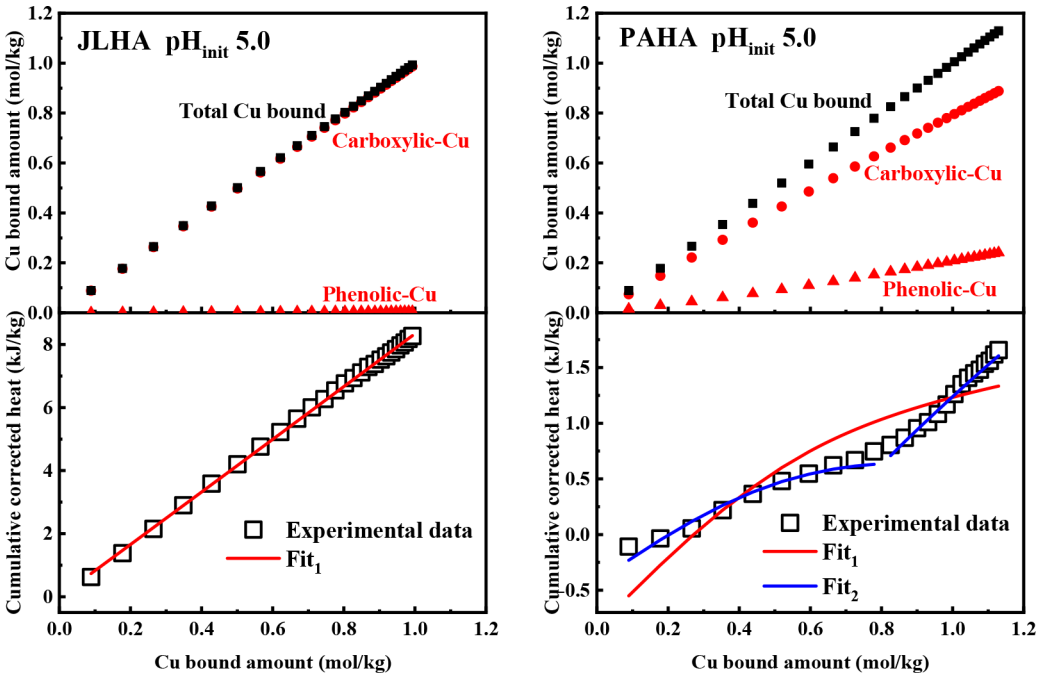


**Figure 3.** Comparison of the adsorption and heat characteristics of JLHA and PAHA at initial pH 5.0 in 0.1 mol/L $KNO_3$. The top panels depict the bound amounts of carboxylic−Cu (solid red spheres), phenolic−Cu (solid red triangles), and total Cu bound (solid black squares) and the bottom panels the cumulative heat corrected by the heat of background and proton exchange (open black squares) as a function of the total amount of $Cu^{2+}$ bound to JLHA and PAHA. The symbols in the bottom panels are the experimental data; the red lines are data fitted ($Fit_1$) with eq 3. The blue lines ($Fit_2$) are refined data fitted with eq 3 that are fitted by making a difference between low and high Cu loadings.



DOI: 10.1021/acs.est.7b06281
Environ. Sci. Technol. 2018, 52, 4099−4107

Table 3. Thermodynamic Parameters for $Cu^{2+}$ Binding to Deprotonated HA[a]

| sample | $pH_{init}$ | species | log $\tilde{k}_{CuLj}$ | $\Delta\bar{G}_{CuLj}$ (kJ/mol) | $\Delta\bar{H}_{CuLj}$ (kJ/mol) | $T\Delta\bar{S}_{CuLj}$ (kJ/mol) |
|---|---|---|---|---|---|---|
| JLHA | 4.0 | carboxylic−Cu | 3.82 | −21.79 | 8.19 | 29.98 |
| | | phenolic−Cu | 8.26 | −47.12 | −19.49 | 27.63 |
| | 5.0 | carboxylic−Cu | 3.82 | −21.79 | 8.54 | 30.33 |
| | | phenolic−Cu | 8.26 | −47.12 | −19.69 | 27.43 |
| PAHA | 4.0 | carboxylic−Cu | 4.65 | −26.53 | 9.80 | 36.33 |
| | | phenolic−Cu | 8.55 | −48.78 | −17.57 | 31.21 |
| | refined | carboxylic−$Cu_{low}$ | – | – | 8.44 | – |
| | | phenolic−$Cu_{low}$ | – | – | −17.44 | – |
| | | carboxylic−$Cu_{high}$ | – | – | 12.03 | – |
| | | phenolic−$Cu_{high}$ | – | – | −17.91 | – |
| | 5.0 | carboxylic−Cu | 4.65 | −26.53 | 7.12 | 33.65 |
| | | phenolic−Cu | 8.55 | −48.78 | −17.45 | 31.33 |
| | refined | carboxylic−$Cu_{low}$ | – | – | 5.92 | – |
| | | phenolic−$Cu_{low}$ | – | – | −17.54 | – |
| | | carboxylic−$Cu_{high}$ | – | – | 9.86 | – |
| | | phenolic−$Cu_{high}$ | – | – | −17.29 | – |

[a]The $\Delta\bar{G}_{CuLj}$, $\Delta\bar{H}_{CuLj}$, and $\Delta\bar{S}_{CuLj}$ represent the average value of, respectively, Gibbs energy, enthalpy, and entropy of Cu binding to deprotonated HA sites of type $j$. The log $\tilde{k}_{CuLj}$ values correspond with affinities of the two peaks in the affinity distribution for Cu. The refined values are the enthalpies that are fitted with eq 3 by making a difference between low and high Cu loadings. The $R^2$ of the fit to obtain the enthalpies is 0.999 for Cu binding to JLHA at $pH_{init}$ 4.0 and 5.0 and 0.977 and 0.848 for Cu binding to PAHA at $pH_{init}$ 4.0 and 5.0, respectively. For the refined fit, $R^2 \geq$ 0.961.

higher affinity of proton binding to phenolic-type sites than carboxylic-type sites.

**3.3. Thermodynamic Parameters for Cu Binding to HA.** The power−time curves obtained for the isothermal titrations of blank and HA solution by the $Cu(NO_3)_2$ solution are presented in Figure S5 (SI). The series of positive peaks reveals that the addition of Cu to HA solution is endothermic at $pH_{init}$ 4.0 and 5.0. The results for the Cu speciation are depicted in the top panels of Figure S6 (SI) ($pH_{init}$ 4.0) and Figure 3 ($pH_{init}$ 5.0). For both JLHA and PAHA, the carboxylic-type sites contribute most to the total Cu binding; for JLHA the contribution of the phenolic-type sites is rather small. The cumulative heats have to be corrected for the increased deprotonation (see eq 3); the corrected heats are depicted in Figure S6 (SI) ($pH_{init}$ 4.0) and Figure 3 ($pH_{init}$ 5.0) in the bottom panels. The obtained curves are fitted to the right-hand side of eq 3 to obtain the site-type-specific average molar enthalpies of Cu binding to *deprotonated* carboxylic- and phenolic-type sites; the results are collected in Table 3 for both samples. Since the small contribution of phenolic-type sites to Cu binding to JLHA leads to a relatively large uncertainty of the corresponding enthalpies, these values are not included in the analysis. It follows that Cu binding to carboxylic-type sites is endothermic (7.12−9.80 kJ/mol), while Cu binding to phenolic-type sites is exothermic (−17.57 and −17.45 kJ/mol).

The site-type-specific average molar Gibbs energies of Cu binding ($\Delta\bar{G}_{CuLj}$, in Table 3) are calculated using the log $\tilde{k}_{CuLj}$. The $\Delta\bar{G}_{CuLj}$ values are all negative because Cu binding is a spontaneous process. With eq 5, $T\Delta\bar{S}_{CuLj}$ is calculated with the known values of $\Delta\bar{G}_{CuLj}$ and $\Delta\bar{H}_{CuLj}$. The resulting $T\Delta\bar{S}_{CuLj}$ values of Cu binding to deprotonated carboxylic- and phenolic-type sites are also listed in Table 3. The positive entropies suggest that Cu binding to deprotonated sites is entropically favorable. A similar driven force is observed for Cu and proton binding to each site-type, which suggests a similar thermodynamic binding mechanism; thus, a high affinity for proton binding also implies a high affinity for Cu binding.

It is worth noting that the fit of Cu-binding enthalpies is poor for PAHA. For JLHA, Cu binding at $pH_{init}$ 4.0 and 5.0 seems to be a simple process in which Cu binding occurs almost exclusively on carboxylic-type sites. For PAHA−Cu, the average site-type-specific enthalpies (one constant value for each site-type) are somewhat crude. Experimental curves show two regions of about constant molar heat for Cu. At $pH_{init}$ 4.0, the first region applies to Cu bound less than 0.51 mol/kg, and the average molar enthalpies for carboxylic- and phenolic-type sites are 8.44 and −17.44 kJ/mol, respectively; the second region applies to high Cu loadings and the average molar enthalpies are 12.03 and −17.91 kJ/mol, respectively. Similarly, the average molar enthalpies at $pH_{init}$ 5.0 are 5.92 and −17.54 kJ/mol at low Cu loadings, and 9.86 and −17.29 kJ/mol at high Cu loadings (>0.82 mol/kg). These results imply that, with Cu binding to PAHA, different complexes form at low and high Cu loadings.

## 4. DISCUSSION

**4.1. Coordination Information Provided by EXAFS.** Previous studies[42,43] have shown that one or two five- to six- or higher membered ring-chelates formed by closely spaced carboxyl and hydroxyl groups are the dominant forms of natural organic matter (NOM)−Cu complexes. The coordination numbers (CN) of 1.7 and 1.9 C in the second shell suggest that the Cu−complexes are mainly represented by one ring in HA with Cu forming bidentate complexes with bridging O functional groups, but because the CN is less than 2, monodentate complexes will also exist. The two rings structure can be less possible due to the relatively low coordination numbers and a larger sterical hindrance for HA with high average molecular weight. The results are in agreement with the stoichiometry ratio, $n_{Cu}/n_H$, of 0.51−0.70 obtained with the NICA model. The closer $n_{Cu}/n_H$ is to 1, the more likely the metal ion is bound as a monodentate complex, and the closer it is to 0.5, the more likely the binding is bidentate.[11,23] Manceau and Matynia[43] have provided the "structure fingerprints" of various coordination modes formed by Cu and functional


DOI: 10.1021/acs.est.7b06281
Environ. Sci. Technol. 2018, 52, 4099−4107

groups of NOM. The six-membered chelate, which has a peak at 2.8 Å $R + \Delta R$ (blue arrow in Figure 1b), is not the dominant species in our HA−Cu samples, since this peak is small for PAHA−Cu and absent for JLHA−Cu in Figure 1b. A second C shell at 3.7−5.0 Å is a characteristic of phthalate−Cu chelate rings or monodentate Cu coordination, which is included in the shadow area in Figure 1b, suggesting that carboxylic−Cu should be significant, which agrees with the NICA calculations. In addition, a strong shoulder between 5.7 and 6.1 $Å^{-1}$ in *k*-space was found in previous studies,[37,38,43] which is a feature of five-membered rings and especially pronounced when Cu is bridging two rings. This shoulder is not obvious in the present study (Figure 1a), and therefore, the structure of two five-membered rings is excluded.

**4.2. Comparison of Thermodynamic Parameters between the HA and Low Molar Mass Organic Acids: H and Cu Coordination.** HAs are complex and heterogeneous assemblages of lower molecular mass components with dominantly carboxylic-type and phenolic-type functional groups.[3,44] The site-type-specific thermodynamic parameters of protonation of HA are compared with those of proton binding to low molar mass organic acids. For some of these acids, the thermodynamic parameters are collected in Table S2 (SI).[45] The values demonstrate that the magnitude of the thermodynamic parameters is related to the structure of the organic acids. Typical enthalpies for proton binding to carboxylic groups of low molar mass organic acids range between −3.8 and 6.02 kJ/mol, and those for phenolic groups range between −20 and −38 kJ/mol. Our measured enthalpies of protonation of the carboxylic-type (0.20 and 0.77 kJ/mol) and phenolic-type sites (−23.61 and −21.41 kJ/mol) are close to, respectively, the carboxylic and phenolic groups of the low molar mass acids. Evidently, proton binding enthalpies of HA are largely determined by the site-type the proton associates with.

The thermodynamic parameters of Cu complexing with organic acids are collected (Table S3, SI).[45] The thermodynamic characteristics are summarized below. When Cu forms monodentate complexes with single-carboxylic ligands, such as acetate, propionate or furanate (A-kind structure in Figure 4), the resulting enthalpies ($\Delta H$ = 4.1−7.1 kJ/mol) and entropies ($T\Delta S$ = 10.7−19.7 kJ/mol) are relatively small. For Cu complexing with dicarboxylic ligands like malonate, succinate, or phthalate, three possible structures exist: monodentate complexes [MHL in Table S3 (SI), B-kind structure in Figure 4], bidentate complexes with single ligand (ML, C-kind structure), bidentate complexes with two separate ligands ($ML_2$, D-kind structure). For the MHL-complex the enthalpies ($\Delta H$ = −0.4−2 kJ/mol) and entropies ($T\Delta S$ = 8.9−12.8 kJ/mol) are even smaller than for the monodentate complexes mentioned above. The enthalpies of ML- and $ML_2$-complexes are comparable and range from 5 to 15 kJ/mol, but the entropies of $ML_2$ ($T\Delta S$ = 46.8−53.3 kJ/mol) are larger than those of ML ($T\Delta S$ = 26.7−37.0 kJ/mol). The enthalpies of Cu binding to the deprotonated carboxylic-type sites of JLHA and PAHA range from 5.92 to 12.03 kJ/mol and the entropies ($T\Delta\overline{S}$) from 29.98 to 36.33 kJ/mol. These thermodynamic parameters of Cu binding to carboxylic-type sites are averages of the diverse carboxylic−Cu configurations. The combination of monodentate complexes and bidentate complexes involving two ligands, or mainly bidentate complexes involving single ligand, could lead to thermodynamic parameters similar to those of Cu binding to carboxylic-type sites of HA. However, the possibility of involving large coordination numbers is not in accordance with the EXAFS results. Therefore, one chelate ring formed by Cu and two carboxylic groups should be the dominant species. Considering this and the various aromatic structures in HA, the C-kind structure provides most likely a large contribution to Cu binding to the carboxylic-type sites. Similarly, the thermodynamic parameters of Cu binding to phenolic-type sites of HA (Table S4; detailed fitting in Figures S7 and S8, SI) are close to those of salicylate and catechol (Table S3, SI). Considering that five- and six-membered rings are not so detectable by EXAFS, phenolic−Cu complexes such as salicylic (E-kind structure, six-membered ring) and catecholic (F-kind structure, five-membered ring) structures should be responsible for the minority of HA−Cu complexes.

The significance of this study is that our understanding of specific ion binding to the different site-types of HS is enhanced by simultaneous use of XAFS, calorimetry, and NICA modeling. The binding behavior of proton and Cu binding to the carboxylic- and phenolic-type HA sites largely depends on the coordination environment, but the thermodynamic driving forces for binding to the carboxylic-type sites are very similar and different from the binding to the phenolic-type sites. Therefore, differences in HA heterogeneity and site densities do not significantly affect the site-type-specific thermodynamic binding mechanisms. This "universal nature" of the site-type-specific thermodynamic parameters, as observed for proton and Cu binding to the two types of functional groups of the two HAs, is of direct importance for the determination of the metal ion binding structures. Most likely, the universal nature of the site-type-specific thermodynamic parameters can also apply to metal ions with a binding mechanism similar to that of Cu in conjunction with chemical speciation models (NICA model in particular), and with EXAFS studies to constrain and/or compare the coordination structures (or stoichiometry indicators) of the chemical speciation model and/or the EXAFS analysis.

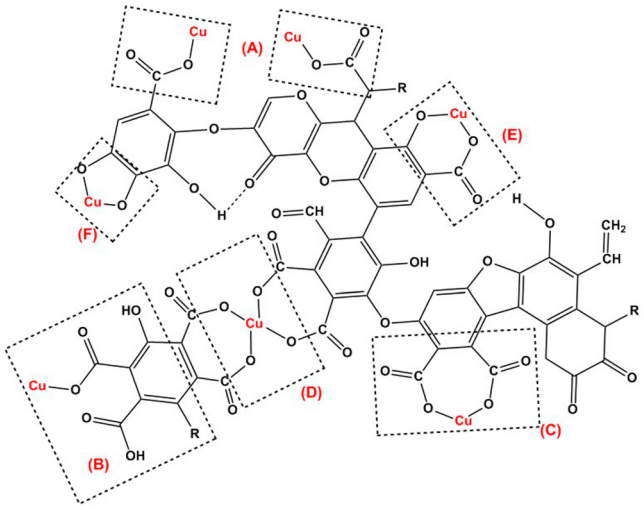


**Figure 4.** Proposed structures for Cu complexes with carboxylic and phenolic groups on HA.

## ■ ASSOCIATED CONTENT

### Supporting Information

The Supporting Information is available free of charge on the ACS Publications website at DOI: 10.1021/acs.est.7b06281.



DOI: 10.1021/acs.est.7b06281
Environ. Sci. Technol. 2018, 52, 4099−4107

NICA model description, additional XAFS methods, and supplementary tables (S1−S4) and figures (S1−S8) (PDF)

## AUTHOR INFORMATION


### Corresponding Authors

*L. C. Fang: e-mail: flinc629@hotmail.com.

*W. F. Tan: e-mail: wenfeng.tan@hotmail.com.

### ORCID

Wenfeng Tan: 0000-0002-3098-2928


### Notes

The authors declare no competing financial interest.

## ACKNOWLEDGMENTS

This work was financially supported by the National Natural Science Foundation of China (Nos. 41425006, 41330852, 41571314, and 41101218), the National Key Basic Research Program of China (No. 2015CB150504), and the CAS "Light of West China" Program (XAB2016A03). We also thank the Beijing Synchrotron Radiation Facility (BSRF) for the valuable beam time.

## REFERENCES


(1) Senesi, N.; Loffredo, E. Metal ion complexation by soil humic substances. In *Chemical Processes in Soils*; Tabatabai, M. A., Sparks, D. L., Eds.; Soil Science Society of America: Madison, WI, 2005; pp 563−618.

(2) Tipping, E. *Cation Binding by Humic Substances*; Cambridge University Press: Cambridge, UK, 2002; Vol. *12*.

(3) Sutton, R.; Sposito, G. Molecular structure in soil humic substances: the new view. *Environ. Sci. Technol.* **2005**, *39* (23), 9009−9915.

(4) Xia, K.; Bleam, W.; Helmke, P. A. Studies of the nature of $Cu^{2+}$ and $Pb^{2+}$ binding sites in soil humic substances using X-ray absorption spectroscopy. *Geochim. Cosmochim. Acta* **1997**, *61* (11), 2211−2221.

(5) Chen, W.; Habibul, N.; Liu, X. Y.; Sheng, G. P.; Yu, H. Q. FTIR and synchronous fluorescence heterospectral two-dimensional correlation analyses on the binding characteristics of copper onto dissolved organic matter. *Environ. Sci. Technol.* **2015**, *49* (4), 2052−2058.

(6) Christl, I.; Milne, C. J.; Kinniburgh, D. G.; Kretzschmar, R. Relating ion binding by fulvic and humic acids to chemical composition and molecular size. 2. Metal binding. *Environ. Sci. Technol.* **2001**, *35* (12), 2512−2517.

(7) Tipping, E.; Hurley, M. A. A unifying model of cation binding by humic substances. *Geochim. Cosmochim. Acta* **1992**, *56* (10), 3627−3641.

(8) Tipping, E.; Lofts, S.; Sonke, J. E. Humic ion-binding Model VII: A revised parameterisation of cation-binding by humic substances. *Environ. Chem.* **2011**, *8* (3), 225−235.

(9) Tipping, E. Humic Ion-Binding Model VI: An improved description of the interactions of protons and metal ions with humic substances. *Aquat. Geochem.* **1998**, *4* (1), 3−47.

(10) Kinniburgh, D. G.; van Riemsdijk, W. H.; Koopal, L. K.; Borkovec, M.; Benedetti, M. F.; Avena, M. J. Ion binding to natural organic matter: competition, heterogeneity, stoichiometry and thermodynamic consistency. *Colloids Surf., A* **1999**, *151* (1-2), 147−166.

(11) Koopal, L. K.; Saito, T.; Pinheiro, J. P.; Riemsdijk, W. H. V. Ion binding to natural organic matter: general considerations and the NICA-Donnan model. *Colloids Surf., A* **2005**, *265* (1−3), 40−54.

(12) Dudal, Y.; Gérard, F. Accounting for natural organic matter in aqueous chemical equilibrium models: a review of the theories and applications. *Earth-Sci. Rev.* **2004**, *66* (3), 199−216.

(13) Merdy, P.; Koopal, L. K.; Huclier, S. Modeling metal-particle interactions with an emphasis on natural organic matter. *Environ. Sci. Technol.* **2006**, *40* (24), 7459−7466.

(14) Orsetti, S.; Andrade, E. M.; Molina, F. V. Modeling ion binding to humic substances: elastic polyelectrolyte network model. *Langmuir* **2010**, *26* (5), 3134−3144.

(15) Kinniburgh, D. G. *Fit, Technical Report WD/93/23*; British Geological Survey: Keyworth, UK, 1993.

(16) Keizer, M. G.; Van Riemsdijk, W. H. *ECOSAT: Equilibrium Calculation of Speciation and Transport*; Wageningen Agricultural University: Wageningen, Netherlands, 1998.

(17) Gustafsson, J. P. *Visual MINTEQ*, version. 3.0; Department of Land and Water Resources Engineering, Royal Institute of Technology: Stokholm, Sweden, 2011.

(18) Meeussen, J. C. ORCHESTRA: an object-oriented framework for implementing chemical equilibrium models. *Environ. Sci. Technol.* **2003**, *37* (6), 1175−1182.

(19) Kinniburgh, D. G.; Milne, C. J.; Benedetti, M. F.; Pinheiro, J. P.; Filius, J.; Koopal, L. K.; Van Riemsdijk, W. H. Metal ion binding by humic acid: application of the NICA-Donnan model. *Environ. Sci. Technol.* **1996**, *30* (5), 1687−1698.

(20) Reycastro, C.; Mongin, S.; Huidobro, C.; David, C.; Salvador, J.; Garcés, J. L.; Galceran, J.; Mas, F.; Puy, J. Effective affinity distribution for the binding of metal ions to a generic fulvic acid in natural waters. *Environ. Sci. Technol.* **2009**, *43* (19), 7184−7191.

(21) Puy, J.; Galceran, J.; Huidobro, C.; Companys, E.; Samper, N.; Garcés, J. L.; Mas, F. Conditional affinity spectra of $Pb^{2+}$-humic acid complexation from data obtained with AGNES. *Environ. Sci. Technol.* **2008**, *42* (24), 9289−9295.

(22) Xu, J.; Tan, W.; Xiong, J.; Wang, M.; Fang, L.; Koopal, L. K. Copper binding to soil fulvic and humic acids: NICA-Donnan modeling and conditional affinity spectra. *J. Colloid Interface Sci.* **2016**, *473*, 141−151.

(23) Koopal, L. K.; van Riemsdijk, W. H.; Kinniburgh, D. G. Humic matter and contaminants. General aspects and modeling metal ion binding. *Pure Appl. Chem.* **2001**, *73* (12), 2005−2016.

(24) Christl, I.; Kretzschmar, R. Relating Ion Binding by Fulvic and Humic Acids to Chemical Composition and Molecular Size. 1. Proton Binding. *Environ. Sci. Technol.* **2001**, *35* (12), 2505−2511.

(25) Saito, T.; Koopal, L. K.; Nagasaki, S.; Tanaka, S. Electrostatic potentials of humic acid: Fluorescence quenching measurements and comparison with model calculations. *Colloids Surf., A* **2009**, *347* (1), 27−32.

(26) Orsetti, S.; Marcobrown, J. L.; Andrade, E. M.; Molina, F. V. Pb(II) binding to humic substances: an equilibrium and spectroscopic study. *Environ. Sci. Technol.* **2013**, *47* (15), 8325−8333.

(27) Prado, A. G.; Airoldi, C. Humic acid-divalent cation interactions. *Thermochim. Acta* **2003**, *405* (2), 287−292.

(28) Qi, Y.; Zhu, J.; Fu, Q.; Hu, H.; Rong, X.; Huang, Q. Characterization and Cu sorption properties of humic acid from the decomposition of rice straw. *Environ. Sci. Pollut. Res.* **2017**, *24* (30), 23744−23752.

(29) Baker, H.; Khalili, F. Comparative study of binding strengths and thermodynamic aspects of Cu (II) and Ni (II) with humic acid by Schubert's ion-exchange method. *Anal. Chim. Acta* **2003**, *497* (1), 235−248.

(30) Swift, R. S. *Methods of Soil Analysis: Part 3, Chemical Methods*; Sparks, D. L., Bartels, J. M., Bigham, J. M., Eds.; Soil Science Society of America: Madison, WI, 1996.

(31) Vermeer, A. W. P.; van Riemsdijk, W. H.; Koopal, L. K. Adsorption of humic acid to mineral particles. 1. Specific and electrostatic interacions. *Langmuir* **1998**, *14* (10), 2810−2819.

(32) Tan, W.; Xiong, J.; Li, Y.; Wang, M.; Weng, L.; Koopal, L. K. Proton binding to soil humic and fulvic acids: experiments and NICA-Donnan modeling. *Colloids Surf., A* **2013**, *436*, 1152−1158.

(33) Ravel, B.; Newville, M. ATHENA, ARTEMIS, HEPHAESTUS: data analysis for X-ray absorption spectroscopy using IFEFFIT. *J. Synchrotron Radiat.* **2005**, *12* (4), 537−541.

(34) Zabinsky, S. I.; Rehr, J. J.; Ankudinov, A.; Albers, R. C.; Eller, M. J. Multiple-scattering calculations of x-ray-absorption spectra. *Phys. Rev. B: Condens. Matter Mater. Phys.* **1995**, *52* (4), 2995−3009.




DOI: 10.1021/acs.est.7b06281
*Environ. Sci. Technol.* 2018, 52, 4099−4107

(35) Biagini Cingi, M. B.; Manotti Landredi, A. M.; Tiripicchio, A.; Tiripicchio Camellini, M. T. The crystal and molecular structures of magnesium di-o-phthalatocuprate(II) tetrahydrate and strontium di-o-phthalatocuprate(II) trihydrate: errata. *Acta Crystallogr., Sect. B: Struct. Crystallogr. Cryst. Chem.* **1979**, *35* (3), 791.
(36) Gorman-Lewis, D.; Fein, J. B.; Jensen, M. P. Enthalpies and entropies of proton and cadmium adsorption onto *Bacillus subtilis* bacterial cells from calorimetric measurements. *Geochim. Cosmochim. Acta* **2006**, *70* (19), 4862−4873.
(37) Strawn, D. G.; Baker, L. L. Molecular characterization of copper in soils using X-ray absorption spectroscopy. *Environ. Pollut.* **2009**, *157* (10), 2813−2821.
(38) Strawn, D. G.; Baker, L. L. Speciation of Cu in a contaminated agricultural soil measured by XAFS, $\mu$-XAFS, and $\mu$-XRF. *Environ. Sci. Technol.* **2008**, *42* (1), 37−42.
(39) Korshin, G. V.; Frenkel, A. I.; Stern, E. A. EXAFS study of the inner shell structure in copper(II) complexes with humic substances. *Environ. Sci. Technol.* **1998**, *32* (18), 2699−2705.
(40) Fang, L.; Zhou, C.; Cai, P.; Chen, W.; Rong, X.; Dai, K.; Liang, W.; Gu, J.-D.; Huang, Q. Binding characteristics of copper and cadmium by cyanobacterium Spirulina platensis. *J. Hazard. Mater.* **2011**, *190* (1), 810−815.
(41) Sheals, J.; Persson, P.; Hedman, B. IR and EXAFS spectroscopic studies of glyphosate protonation and copper(II) complexes of glyphosate in aqueous solution. *Inorg. Chem.* **2001**, *40* (17), 4302−4309.
(42) Karlsson, T.; Persson, P.; Skyllberg, U. Complexation of copper (II) in organic soils and in dissolved organic matter-EXAFS evidence for chelate ring structures. *Environ. Sci. Technol.* **2006**, *40* (8), 2623−2628.
(43) Manceau, A.; Matynia, A. The nature of Cu bonding to natural organic matter. *Geochim. Cosmochim. Acta* **2010**, *74* (9), 2556−2580.
(44) Matynia, A.; Lenoir, T.; Causse, B.; Spadini, L.; Jacquet, T.; Manceau, A. Semi-empirical proton binding constants for natural organic matter. *Geochim. Cosmochim. Acta* **2010**, *74* (6), 1836−1851.
(45) Smith, R.; Martell, A.; Motekaitis, R. NIST standard reference database 46. *NIST Critically Selected Stability Constants of Metal Complexes Database*, version 8; NIST: Gaithersburg, MD, 2004; 2.


DOI: 10.1021/acs.est.7b06281
*Environ. Sci. Technol.* 2018, 52, 4099−4107